Modeling Fission Dynamics
with Leadership Class Computing Capabilities

I. Stetcu[a], A. Bulgac[b], S. Jin[b], K. J. Roche[b,c] and N. Schunk[d]

[a] *Los Alamos National Laboratory, Los Alamos, New Mexico, 87545, USA*

[b] *University of Washington, Seattle, Washington 98195-1560, USA*

[c] *Pacific Northwest National Laboratory, Richland, Washington 99352, USA*

[d] *Lawrence Livermore National Laboratory, Livermore, California 94551, USA*

Abstract

In this contribution, we present a snapshot of recent progress in the microscopic description of low-energy nuclear fission using the time-dependent density functional theory approach, made possible by the latest advances in computational infrastructure. Independent of the choice of the nuclear energy density functional, our investigations show that the collective motion is highly dissipative, with little trace of inertial dynamics, due to the one-dissipation mechanism alone. This finding justifies the validity of using the overdamped collective motion approach. We also briefly discuss the inclusion, in a quantum-mechanical unitary approach, of fluctuations and dissipation. These two components are indispensable to the description of observed distributions (e. g., mass, charge, total kinetic energy). Thus, as the next generation leadership-class computers are being deployed, the fully microscopical description of fission observables and their distributions is within reach.

Keywords: *Fission; density functional theory*

1   Introduction

Two major developments in theory and computational resources created the favorable conditions for achieving a microscopic description of nuclear fission almost eighty years after its discovery in 1939 by Hahn and Strassmann [1]. The density functional theory (DFT) provides the only microscopic framework suitable for description of heavy nuclei and feasible on today's computers. Instead of computing the full many-body wave function, one can determine only the one-body density within the DFT, the highly successful approach pioneered by Kohn, Hohenberg and Sham [2, 3] for many-electron systems in chemistry and condensed matter physics. Within the extension to time-dependent DFT [4–6], the fission dynamics becomes computationally manageable and, hence, a microscopic description feasible. To study quantum dynamics, we implemented on leadership class computers the real-time DFT extension, explicitly including the dynamics of the crucial pairing correlations [6]. At the moment, we are concentrating on obtaining average properties of fission fragments (FFs)

produced during the process, before neutron, gamma and beta emissions, with a plan to describe distributions of relevant observables in the near future. The broad goals of our investigations are to provide a microscopic understanding of the fission process, and to help guide other models used in applications.

In practical applications ranging from energy production to global security, understanding and accurately predicting the distribution of prompt neutron and gamma observables is essential. Hence, phenomenological codes, like FREYA [7] at Livermore and CGMF [8,9] at Los Alamos, have been developed. In such approaches, the fission fragments are treated as compound nuclei, whose de-excitation via neutron and gamma emission can be modeled using Weisskopf [10] or Hauser–Feshbach [11] formalisms. Input into these models usually comes from direct experimental data, like measured mass, charge and total kinetic energy distributions. However, for other important input quantities, only indirect information can be extracted. For example, if one can compute the total excitation energy available in FFs from the energy balance of the reaction, an additional information on the number of neutrons emitted as a function of the FF mass has been used in order to parameterize the total energy sharing between FFs. This type of data is available for a limited number of reactions, usually spontaneous fission of select actinides and fission induced by thermal neutrons. Much fewer data are available at higher incident neutron energies, although the existing data [12] illustrates an interesting property: the entire additional excitation energy brought by the neutron is stored in the heavy fragment. Current modeling capabilities do not take this feature into account given the lack of experimental data necessary to parameterize the energy dependence.

The FF spin distributions are important in the description of prompt gamma properties. A direct measurement of the angular momenta cannot be performed, but model-dependent attempts to extract average values have been made in the past from other fission observables like isomer production ratios [13, 14], gamma-ray de-excitation feeding patterns of the ground-state bands [15] and angular anisotropy of prompt-fission gamma rays [16]. The information such experiments provide is sparse, often limited to even-even isotopes. In addition, even for a simple case of thermal neutron capture, the simulations do not produce an excellent agreement with experimental data [17].

Existing theoretical models of fission based on random-walks on an energy surface [18], Langevin approach with fluctuations and dissipation [19], or more microscopic approaches like DFT + time-dependent generator coordinator method [20] do not produce fully separated FFs and can be plagued by the adiabatic approximation, which inherently produces "cold" fragments. Our time-dependent superfluid local density approximation (TD-SLDA) is the only framework in which the FFs can be fully separated, and an important information (e. g., the energy sharing or FF spins) could be extracted. Such simulations require significant computational resources, but can be also useful in providing microscopic support for existing theoretical approaches to fission, that can be more practical in the sense of requiring limited computational power.

In this contribution, we review our previous investigations of the fission of the ^{240}Pu nucleus. Since the TD-SLDA can only provide average quantities, we briefly discuss introducing fluctuations and dissipations in the evolution, so that the full distributions can be calculated in the near future.

2 Theoretical framework

In mean-field theories, the ground state of a quantum system is described by a single Slater determinant, constructed from particle states for closed-shell nuclei or quasi-particle states for open-shell nuclei. Densities and current densities are computed from this single Slater determinant, and the ground state energy is computed by minimizing a density energy functional, which is formally equivalent to solving the self-consistent Hartree–Fock–Bogoliubov or Bogoliubov–de Gennes equations for the (quasi-)particle wave functions:

$$
\begin{pmatrix}
h_{\uparrow\uparrow} - \mu & h_{\uparrow\downarrow} & 0 & \Delta \\
h_{\downarrow\uparrow} & h_{\downarrow\downarrow} - \mu & -\Delta & 0 \\
0 & -\Delta^* & -(h_{\uparrow\uparrow}^* - \mu) & -h_{\uparrow\downarrow}^* \\
\Delta^* & 0 & -h_{\downarrow\uparrow}^* & -(h_{\downarrow\downarrow}^* - \mu)
\end{pmatrix}
\begin{pmatrix}
u_{k\uparrow} \\
u_{k\downarrow} \\
v_{k\uparrow} \\
v_{k\downarrow}
\end{pmatrix}
= E_k
\begin{pmatrix}
u_{k\uparrow} \\
u_{k\downarrow} \\
v_{k\uparrow} \\
v_{k\downarrow}
\end{pmatrix},
\qquad (1)
$$

where $u_{k\uparrow(\downarrow)}$ and $v_{k\uparrow(\downarrow)}$ are the up (down) components of the quasiparticle wave functions (qpwfs), with the dependence on the spacial coordinates not shown explicitly, E_k is the corresponding quasiparticle energy, and μ is the chemical potential needed to impose a constraint on the desired number of particles. The one-body Hamiltonian h is a function of the densities and current densities and can include external fields (and, in particular, additional constraints). The superfluid local density approximation (SLDA) reduces Eq. (1) to the usual Hartree–Fock equations when the pairing field is zero (the so-called normal systems). In the case of nuclear systems, two different coupled equations, one for protons and one for neutrons, need to be solved.

The dynamics is obtained by following in time the evolution of the qpwfs by solving the time-dependent Schrödinger-like equations,

$$
i\hbar \frac{\partial}{\partial t}
\begin{pmatrix}
u_{k\uparrow} \\
u_{k\downarrow} \\
v_{k\uparrow} \\
v_{k\downarrow}
\end{pmatrix}
=
\begin{pmatrix}
h_{\uparrow\uparrow} - \mu & h_{\uparrow\downarrow} & 0 & \Delta \\
h_{\downarrow\uparrow} & h_{\downarrow\downarrow} - \mu & -\Delta & 0 \\
0 & -\Delta^* & -(h_{\uparrow\uparrow}^* - \mu) & -h_{\uparrow\downarrow}^* \\
\Delta^* & 0 & -h_{\downarrow\uparrow}^* & -(h_{\downarrow\downarrow}^* - \mu)
\end{pmatrix}
\begin{pmatrix}
u_{k\uparrow} \\
u_{k\downarrow} \\
v_{k\uparrow} \\
v_{k\downarrow}
\end{pmatrix},
\qquad (2)
$$

where, for simplicity, in addition to the spatial coordinate $\vec{r}$, we have also suppressed the time coordinate t. At each time t, the one-body Hamiltonian and the pairing field depend on the densities and currents constructed from the qpwfs at the same time t.

The TD-SLDA can treat both linear response (equivalent to QRPA) and large amplitude collective motion (e. g., fission). However, during the time evolution, the underlying solutions are single Slater determinants, even in the case of fission shown in Fig. 1, when two fragments are formed. In DFT, in general, densities are the quantities of interest and not the many-body wave functions.
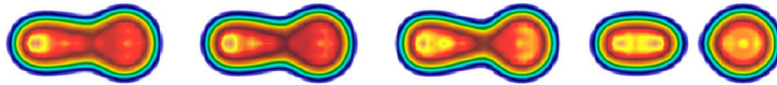

Figure 1: Evolution from a compact configuration to one where the two fragments are fully separated.

3 Numerical details

In our implementation, both the SLDA and TD-SLDA equations (1) and (2) are discretized on rectangular lattices, the former providing initial conditions for the latter. While the dimensions of the matrices involved are very large, this discretization allows us to obtain solutions without any symmetry restrictions (arbitrary deformations) and to describe accurately the continuum components of the qpwfs.

Less demanding numerical methods that allow the extraction of densities and currents without the full diagonalization of Eq. (1) exist. We have implemented one such method efficiently on GPU machines [21]. However, in order to start the time evolution, the full initial eigenvector is required at $t = 0$. Therefore, the initial qpwfs are obtained by a full diagonalization of the HFB matrix, using the package SCALapack. Assuming N_x, N_y and N_z lattice points in x, y and z directions respectively, the basis states used to diagonalize the full HFB matrix are given generically by

$$\Phi_{i_x,i_y,i_z}(\vec{r}) = \phi_{i_x}(x)\,\phi_{i_y}(y)\,\phi_{i_z}(z), \tag{3}$$

where

$$\phi_{i_x}(x) = \frac{1}{N}\,\exp\!\left(-\frac{i\pi(x - x_{i_x})}{dx}\right)\frac{\sin\frac{\pi(x-x_{i_x})}{dx}}{\sin\frac{\pi(x-x_{i_x})}{N_x dx}}, \tag{4}$$

with dx being the lattice constant in x direction and $i_x = 0, \ldots, N_x - 1$ is the location on the lattice, and similarly for the y and z directions. Each component is expanded using the basis states (3), so that the total dimension is $4N_xN_yN_z$. The matrix elements of all operators can be analytically calculated in this basis. Because of the spin-orbit contribution, the matrix in Eq. (1) is complex Hermitian. Note that the phase factor included in Eq. (4) is necessary to ensure compatibility with the fast Fourier transforms computed with the FFTW package (on CPUs or its cuda implementation). This discrete variable representation basis is optimal for numerically representing wave functions in nuclear physics [22], and SLDA in particular.

The time evolution of the nuclear system formally represented by Eq. (2) is simulated using the fifth order Adams–Bashford–Milne numerical method [23]. This approach reduces the number of applications of the Hamiltonian at each time step to only two, although the errors are of the order $\mathcal{O}(\Delta t^5)$, where Δt is the numerical integration step in time. The derivatives are efficiently calculated via Fourier transforms, using GPU accelerators. It is well know that on systems with GPUs, the bottleneck could be the need to transfer often large amounts of data between CPUs and GPUs. We minimize the amount of data exchanged by only transferring the densities for reduction over CPUs using MPI calls. This ensures almost perfect weak and strong scaling properties. At this moment, the bottleneck for the time-dependent code is only restricted by the communications between MPI processes. We will publish a more detailed analysis of the scaling properties of the code in an upcoming manuscript, which will accompany the release of both the static and dynamic codes as open sources. The advantage brought by GPU acceleration is remarkable, providing a speedup factor of 9.4x with respect to the CPU version only of the code, when the two are compared on the same number of processors. The CPU and hybrid CPU+GPU versions of the codes have the same design, the only difference being the use of GPUs to accelerate numerically intensive portions of the code, like the time integration and calculation of densities. Compared with other time dependent

state-of-the-art codes in the literature, our simulations solve three to four orders of magnitude more partial differential equations, being about 100 times faster than other approaches. This significant improvement over other simulations is a consequence of the less demanding while accurate time-integration algorithm, as well as the efficient use of GPUs to accelerate the calculations, in particular, the use of accurate Fast Fourier transforms for spatial derivatives. The first application of these codes have been to linear response [24] and relativistic Coulomb excitation of heavy nuclei [25], but the main focus of our work has been devoted to fission.

The evolution in time follows the system from a compact shape to two fully separated fragments. When the fragments are fully separated, we split the box into two, and compute the properties of each fragment in its half of the box. The total kinetic energy (TKE) is calculated by adding each FF kinetic energy and the Coulomb interaction between the fragments, as TKE is defined at infinite distance between fragments. We can also compute the total energy of each fragment, and then calculate the FF excitation energy by subtracting the ground state energy computed in an independent minimization for each FF.

4   Fission fragment properties from fission dynamics

In our first simulations of the fission of ^{240}Pu [26], our initial states in the evolution were chosen from beyond the fission barrier, a few MeVs above the zero-temperature potential energy surface. Those states were obtained with a mix of shape constraints and external potentials that would induce a mass asymmetry. The constraints and external potential were then removed adiabatically, and the dynamics of the system followed from a compact initial configuration to two fully separated fragments, as shown in Fig. 1. For this first calculation, the SLy4 parameterization of the Skyrme functional was chosen. However, because the potential energy surface and the fission barrier properties in particular are not well described with this functional, it was found that the evolution time from the saddle to the scission can be extremely large [26] as this particular functional facilitates the conversion between multiple collective degrees of freedom. It was also found that the saddle-to-scission time is particularly sensitive to the pairing correlations, which is to be expected as the pairing interaction facilitates fission at low energies [27–29]. Finally, results obtained in TD-SLDA are consistent with expectations that the light fragment emerges deformed, while the heavy fragment is close to spherical shape with very weak or collapsed pairing field, as it is expected to be close to a closed shell configuration.

In Ref. [26], only four distinct initial conditions have been used to compute the FF properties. Hence, one of natural and frequently asked questions was about the impact the particular initial conditions have on the final results. In a more recent investigation of Ref. [30], we have started with a larger number of initial conditions considering different points on the potential energy surface. In this case, we have used functionals that better describe the potential energy surfaces of actinides, in particular, the SKM* and recently developed SeaLL1 density functionals. The initial conditions were chosen to have a large spread in quadrupole deformation (Q_{20}) and mass asymmetry (Q_{30}), but similar initial excitation energies with respect to the ground state, as shown in Fig. 2. The two sets of initial conditions shown in Fig. 2 have excitation energies around 7.9 MeV (red) and 2.6 MeV (blue), respectively.

The results of the two sets of calculations are summarized in Table 1. Despite the
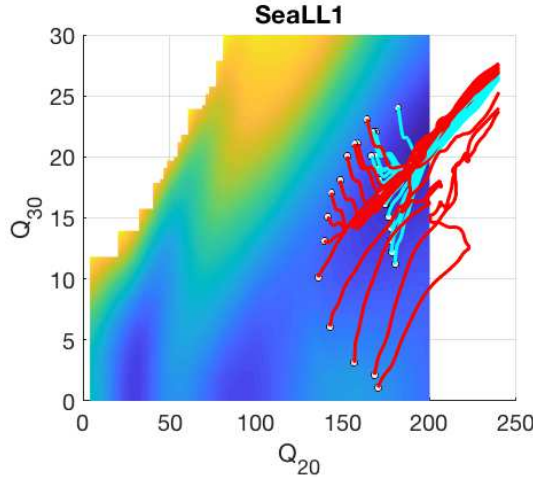
Figure 2: Evolution from compact to separated shapes in the (Q_{20}, Q_{30}) plane, for the SeaLL1 nuclear density functional. These trajectories start around 7.9 MeV (red) and 2.6 MeV (blue) excitation energies, with a standard deviation of about 1.7 and 1.8 MeV, respectively. Q_{20} is in the units of b and Q_{30} is in the units of $b^{3/2}$.

relatively large spread in the shape of the initial state, the fragments are produced with a relatively small dispersion in all observables, as illustrated by the focusing of the different trajectories in Fig. 2. The TD-SLDA can only provide an average path for the evolution, following to a large extent the minimum on the potential energy surface. Very similar FF characteristics are thus obtained within TD-SLDA, if no fluctuations (and dissipation) are included.

An interesting feature of the evolution is the fact that the collective energy flow, defined as

$$E_{\text{coll.flow}} = \int d^3\vec{r}\, \frac{\vec{j}^2(\vec{r}, t)}{2M_N \rho(\vec{r}, t)}, \tag{5}$$

where $\vec{j}(\vec{r}, t) = \frac{i\hbar}{2} \sum_k \left(v_k^*(\vec{r}, t)\vec{\nabla} v_k(\vec{r}, t) - v_k(\vec{r}, t)\vec{\nabla} v_k^*(\vec{r}, t) \right)$ is the current density, and $\rho(\vec{r}, t) = \sum_k |v_k(\vec{r}, t)|^2$ is the particle number density, remains almost constant throughout the saddle-to-scission evolution, and at a very low (1–2 MeV) value. Hence, the motion from the saddle to the scission is strongly dissipative, because the one-body dissipation included in TD-SLDA is strong. This finding is at odds with adiabatic approaches, where one expects a full conversion of the collective energy potential surface into a collective flow energy of about 15 to 20 MeV from the saddle to the scission, and in line with the hypothesis of overdamped collective motion, as assumed in the work by Randrup *et al.* [31].

Fluctuations and dissipations have been introduced recently in a quantum-mechanical fully-unitary approach [32]. The fluctuations are modeled by introducing

Table 1: The excitation energy of the initial state used in TD-SLDA evolution, TKE, charge, mass and excitation energy of the heavy FF for the trajectories shown in Fig. 2. We record the standard deviation for each quantity in parentheses.

E_{ini}^* (MeV)	TKE (MeV)	Z_H	A_H	E_H^* (MeV)
7.9(1.7)	177.8(3.1)	53.2(0.4)	136.6(0.8)	17.1(3.0)
2.6 (1.8)	178.0(2.3)	52.9(0.4)	135.8(0.6)	19.5(3.8)

a "stochastic" velocity field $\vec{u}(\vec{r}, t)$, see Ref. [32] for details. This additional field induces heating in the system, which has to be counterbalanced by a dissipation term to the evolution of the form $\gamma[\rho(\vec{r}, t)]\dot{\rho}(\vec{r}, t)$, with a density-dependent strength γ. This addition ensures that the energy of the system is conserved on average. The strength of the friction term is connected to the strength of the stochastic field, similar to the Einstein's fluctuation-dissipation theorem.

The resources necessary to run simulations that include fluctuations and dissipation in TD-SLDA are considerable. Hence, for the first test that also allow us to experiment with the strength of fluctuation and dissipation terms, this approach has been implemented in the nuclear quantum hydrodynamic equations using a phenomenological nuclear energy density functional [32]. The hydrodynamic equations do not include the shell effects and stationary states with broken left-right symmetry have always higher energies than states with unbroken left-right symmetry. In applications to the spontaneous fission of ^{258}Fm, the widths of the simulated distributions are in good agreement with observed experimental distributions [32]. The fluctuations and dissipation have been also implemented in the full TD-SLDA equations and illustrated in Ref. [32]. Calculations of the full distribution of fission observables are thus within reach, even with the current computational power available on leadership capabilities available today (and in the near future).

5   Conclusions

Current computing capabilities put us in the position to be able to envision a complete microscopic model for fission in the next few years. TD-SLDA is an effective tool in answering qualitative and quantitative questions regarding the dynamics of the fission process. This is also the only method that can offer a guidance on properties that simply cannot be described in alternate approaches. This includes the excitation energy sharing mechanism between the fission fragments and its behavior with increasing the incident neutron energy. Within the TD-SLDA one can also investigate the physics of scission neutrons, that make the subject of heated debate in the community, and the distribution of the angular momenta. In the future, we will obtain trends with the incident energy of the incoming neutrons from TD-SLDA calculations and will use them as an input in phenomenological calculations of prompt fission neutron and gamma-ray emission.

Acknowledgments

References

[1] O. Hahn and F. Strassmann, Naturwis. **27**, 11 (1939).

[2] P. Hohenberg and W. Kohn, Phys. Rev. **136**, B864 (1964).

[3] W. Kohn and L. J. Sham, Phys. Rev. **140**, A1133 (1965).

[4] E. Runge and E. K. U. Gross, Phys. Rev. Lett. **52**, 997 (1984).

[5] L. N. Oliveira, E. K. U. Gross and W. Kohn, Phys. Rev. Lett. **60**, 2430 (1988).

[6] A. Bulgac, Annu. Rev. Nucl. Part. Sci. **63**, 97 (2013).

[7] J. Verbeke, J. Randrup and R. Vogt, Comput. Phys. Commun. **222**, 263 (2018).

[8] B. Becker, P. Talou, T. Kawano, Y. Danon and I. Stetcu, Phys. Rev. C **87**, 014617 (2013).

[9] P. Talou, T. Kawano and I. Stetcu, *CGMF documentation. Tech. rep. LA-UR-14-24031.* Los Alamos National Laboratory, Los Alamos, 2014.

[10] J. M. Blatt and V. F. Weisskopf, *Theoretical nuclear physics.* Wiley, New York, 1952.

[11] W. Hauser and H. Feshbach, Phys. Rev. **87**, 366 (1952).

[12] A. A. Naqvi, F. Käppeler, F. Dickmann and R. Müller, Phys. Rev. C **34**, 218 (1986).

[13] S. S. Kapoor and R. Ramanna, Phys. Rev. **133**, B598 (1964).

[14] H. Naik, S. P. Dange and R. J. Singh, Phys. Rev. C **71**, 014304 (2005).

[15] J. B. Wilhelmy, E. Cheifetz, R. C. Jared, S. G. Thompson, H. R. Bowman and J. O. Rasmussen, Phys. Rev. C **5**, 2041 (1972).

[16] M. M. Hoffman, Phys. Rev. **133**, B714 (1964).

[17] I. Stetcu, P. Talou, T. Kawano and M. Jandel, Phys. Rev. C **88**, 044603 (2013).

[18] P. Möller, D. G. Madland, A. J. Sierk and A. Iwamoto, Nature **409**, 785 (2001).

[19] A. J. Sierk, Phys. Rev. C **96**, 034603 (2017).

[20] N. Schunck and L. M. Robledo, Rep. Prog. Phys. **79**, 116301 (2016).

[21] S. Jin, A. Bulgac, K. Roche and G. Wlazłowski, Phys. Rev. C **95**, 044302 (2017).

[22] A. Bulgac and M. M. Forbes, Phys. Rev. C **87**, 051301(R) (2013).

[23] R. W. Hamming, *Numerical methods for scientists and engineers*. Dover, 1986.

[24] I. Stetcu, A. Bulgac, P. Magierski and K. J. Roche, Phys. Rev. C **84**, 051309(R) (2011).

[25] I. Stetcu, C. A. Bertulani, A. Bulgac, P. Magierski and K. J. Roche, Phys. Rev. Lett. **114**, 012701 (2015).

[26] A. Bulgac, P. Magierski, K. J. Roche and I. Stetcu, Phys. Rev. Lett. **116**, 122504 (2016).

[27] G. F. Bertsch, F. Barranco and R. A. Broglia, in *Windsurfing the Fermi sea: Proc. Int. Conf. and Symposium on Unified Concepts of Many-Body Problems in honor of Gerry Brown's 60th birthday, September 4–6, 1986, Stony Brook, USA*, eds. T. T. S. Kuo and J. Speth. North-Holland, Amsterdam, 1987, p. 33.

[28] F. Barranco, R. A. Broglia and G. F. Bertsch, Phys. Rev. Lett. **60**, 507 (1988).

[29] G. F. Bertsch and A. Bulgac, Phys. Rev. Lett. **79**, 3539 (1997).

[30] A. Bulgac, S. Jin, K. J. Roche, N. Schunck and I. Stetcu, Phys. Rev. C **100**, 034615 (2019).

[31] J. Randrup, P. Möller and A. J. Sierk, Phys. Rev. C **84**, 034613 (2011).

[32] A. Bulgac, S. Jin and I. Stetcu, Phys. Rev. C **100**, 014615 (2019).